

# 1 Introduction and Motivation

We propose a new experiment to look for a hypothetical dark matter particle known as the *dark photon*, also called the  $A'$ . Although dark matter is typically assumed to be noninteracting, a feeble analog of the standard model electromagnetic interaction could be active in the dark sector, and its photon – the dark photon – could be produced in  $e^+e^-$  annihilations. The experiment we propose can be built and run in a 3-year funding period for modest cost, and it will extend the current limits in dark photon parameter space by almost two orders of magnitude. Using the 5.3 GeV positron beam at Cornell’s Wilson Laboratory the experiment will search for  $e^+e^- \rightarrow \gamma A'$  [1], reconstructing the dark photon mass with a missing mass technique that depends only on the  $e^+$ ,  $e^-$ , and  $\gamma$  kinematics. No assumptions about the  $A'$  decay mode need be made. The detector will be constructed primarily from components recovered at zero cost from the retired CLEO and Babar experiments. The proposed experiment will be referred to here as the “Missing-Mass A-Prime Search”, or MMAPS.

The proponents include faculty from Cornell (Alexander, Perelstein, Rubin, and Wittich) and from Minnesota (Kubota), as well as APEX experiment spokesperson Wojtsekhowski [1–3], representing expertise in experimental particle physics, accelerator physics, and particle theory.

**Changes since 2014.** Since a previous submission in 2014, the experimental design in this proposal has evolved substantially. Key changes include: beryllium target (not  $\text{LH}_2$ ); all-vacuum expansion volume; phototubes replace photodiodes for much-improved pileup handling; improved algorithms for decomposing PMT waveforms with pileup; beam diagnostics in external beamline; three-septum extraction design; ferrite rather than steel quadrupoles and sextuple for enhanced agility; and many additional refinements to designs. In addition, new experimental measurements of synchrotron tune, readout and DAQ electronics, phototubes and photodiodes, and CsI crystals confirm anticipated performance and lend confidence to the predictions made here.

## 1.1 Intellectual Merit

Many theoretical extensions of the Standard Model (SM), such as supersymmetric models and string theories, contain “dark sectors”, consisting of particles with strongly suppressed interactions with the SM fields. Dark sectors are also motivated by cosmological observations, which indicate that about 80% of matter in the Universe consists of dark matter. While the SM contains no good candidate particle for dark matter, it can arise naturally in models with dark sectors, if one or more of the new states are stable on cosmological time scales. Given the rich structure of the SM, it would not be surprising if dark matter is accompanied by a similarly rich set of particles and interactions, all hidden from the SM due to their small couplings to it. Such particles may have masses well below the current high-energy frontier explored by the LHC, as long as their SM interactions are sufficiently small to have escaped discovery thus far.

The recent P5 report [4] identifies the topics under study in this proposal as two of the five ‘science drivers’ for the future of particle physics: namely, to “identify the new physics of dark matter”; and to “explore new particles, interactions, and physical principles”. The P5 report finds it “imperative to search for dark matter along every feasible avenue” and urges that the US physics program “probe dark matter interactions with ordinary matter over a range of dark matter masses and interaction types, with large and important discovery reach (2015-2024).” Its recommendations also call for support for “mid- and small-scale projects”.

In this proposal, we discuss a search for a dark photon, a massive gauge boson of the dark sector. (For a recent review, see Ref. [5].) A dark photon  $A'$  would form a natural portal between the SM and the dark sector, since a renormalizable kinetic mixing term in the Lagrangian can effectively

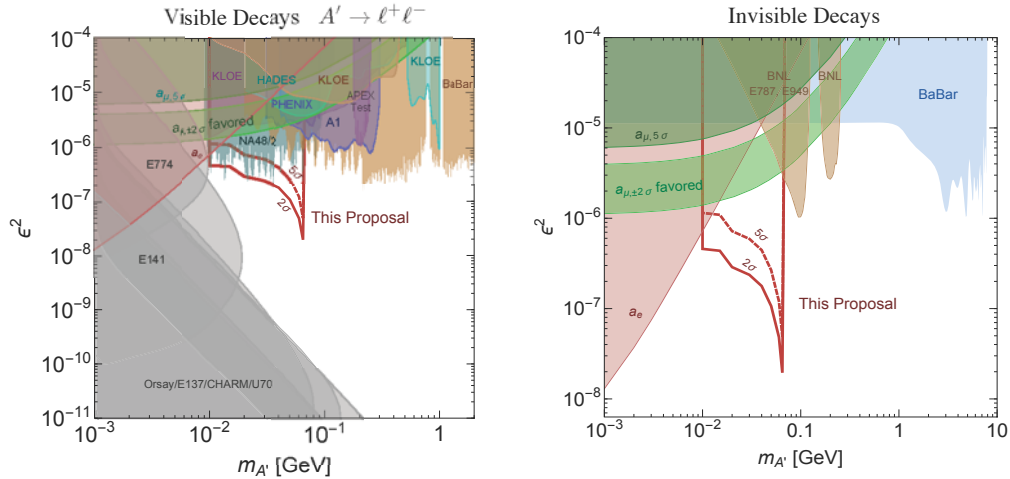


Figure 1: Current experimental bounds [9, 10] on the dark photon mass  $M_{A'}$  and the square of the coupling constant to electrons and positrons,  $\epsilon^2$ . Left panel: experiments sensitive to the *visible*  $A' \rightarrow e^+e^-$  final state. Right panel: experiments sensitive to *invisible*  $A'$  decays.

couple it to the SM electric current:

$$\mathcal{L}_{\text{int}} = \epsilon e A'_\mu J_{\text{EM}}^\mu, \quad (1)$$

where  $\epsilon$  is a dimensionless parameter. Theory does not make a definitive prediction for  $\epsilon$ : values in the broad range  $\epsilon \sim 10^{-12} - 10^{-2}$  have been discussed. The dark photon has been invoked [6] to explain the discrepancy of the anomalous magnetic moment of the muon measured by the E821 experiment [7] with the SM prediction. The correction to  $(g - 2)_\mu$  from the dark photon loops is of the right size to account for the discrepancy if the dark photon mass is below 1 GeV, and  $\epsilon \sim 10^{-3} - 10^{-2}$ . The dark photon also plays a crucial role in the dark matter interpretation of the excess in high-energy positron flux observed by the PAMELA, FERMI and AMS-02 collaborations [8], and points to a mass range of 1 – 200 MeV.

Several experimental searches for dark photons have been conducted in the last few years; see Fig. 1 for a summary of the current experimental situation. Most experiments rely on the EM coupling of the dark photon, Eq. (1), as the main production mechanism. The search strategy then depends on the dark photon decay pattern. A dark photon in the interesting mass range can decay into an  $e^+e^-$  pair. Several experiments such as APEX [2], A1 [11], and NA48 [12] used this final state. Assuming a 100% branching fraction, the region where  $(g - 2)_\mu$  anomaly can be explained is now completely ruled out for the visible case where the decay  $A' \rightarrow e^+e^-$  is reconstructed. An alternative possibility is that the dark photon decays into a pair of dark sector states, which are unobserved. Such invisible decays can naturally have large branching ratios, since while  $\Gamma(A' \rightarrow e^+e^-)$  is suppressed by  $\epsilon^2$ , the dark photon couplings to other dark sector states can be unsuppressed. In this case, the best limits are set by the BaBar search for  $e^+e^- \rightarrow \gamma + \text{invisible}$  [13], and by rare kaon decay experiments at BNL. [14, 15] If the structure of the dark sector is even richer, most existing bounds can be evaded [16].

The dark photon search described here has two key advantages. First, within the accessible dark photon mass window (10 – 70 MeV), it will probe values of  $\epsilon^2$  in the range  $10^{-6} - 10^{-8}$ , significantly extending the reach of the current generation of experiments (see Fig. 1). Second, the proposed experiment uses the missing-mass technique to place bounds that are *completely independent* of the

dark photon decay pattern [1]. Two other similar experiments [17, 18] have just been approved; both are limited to 10 times lower beam energy and reach dark photon masses in the 5-20 MeV range; our mass coverage neatly complements these other experiments. The MMAPS reach shown in Fig. 1 assumes statistical errors dominate and systematic errors can be controlled to the needed level with the calibration techniques discussed in Sec. 4.4. The reach curve reflects local significance only; look-elsewhere effects will be included if any signal candidate appears.

## 1.2 Experimental Strategy

In the MMAPS experiment we will search for the process  $e^+e^- \rightarrow \gamma A'$  in events produced by a positron beam incident on a fixed target. The ordinary photon in the final state is observed and its four-momentum measured; with a sufficiently large dataset the unseen  $A'$  will appear as a bump in the missing-mass spectrum,  $M_{\text{miss}}^2 \equiv (p_{e^+} + p_{e^-} - p_\gamma)^2$ .

**Figure of Merit.** The figure of merit for a bump-hunting experiment is the sensitivity  $S/\sqrt{B}$  at any bump mass  $M_{\text{miss}}$ . For luminosity  $\mathcal{L}$ , runtime  $T$ , and mass resolution  $\sigma_M$ , the figure of merit for an apparatus of acceptance  $\mathcal{A}$  can be defined as F.O.M.  $\equiv \sqrt{\mathcal{L}T\mathcal{A}}/\sigma_{M\text{rec}}$ . The experimental goals are therefore, in broad-brush terms, to obtain the highest possible beam intensity, the highest practical acceptance, and the lowest possible mass resolution.

**Unique Accelerator Facilities.** MMAPS can be realized at Cornell’s Wilson Lab where the existing synchrotron provides a positron source with properties well-matched to the goals of this experiment. A comparable positron beam is not available elsewhere in the world. The positrons will be extracted slowly from the synchrotron over an energy range around 5.3 GeV and directed to a fixed target; the main detector element, a calorimeter of CsI crystals, is positioned 10 m farther downstream. Figures 3 and 7 illustrate the planned location and configuration of the detector. Dismantling of the CLEO iron and rearrangement of radiation shielding is already in progress to accommodate the apparatus. A small number of magnets need to be designed and fabricated to extract the positron beam from the synchrotron, and some vacuum work is needed when we reposition the existing synchrotron magnets to accommodate new elements. These are routine tasks for the Laboratory, well within the capabilities of the experienced accelerator and technical staff.

**Available Detector Components.** Most of the detector components will be adapted from existing equipment inherited from previous experiments. The CsI crystals are taken from the now-retired CLEO experiment, and many of the accelerator components already exist and require only reconfiguration or other limited modifications. For improved performance, the photodiodes used to readout the CLEO calorimeter will be replaced by phototubes from the now-retired Babar DIRC. Four thousand Babar phototubes are currently in storage at Jefferson Lab, and the lab has agreed to provide 1200 for this experiment. The availability of the CLEO CsI and Babar phototubes saves an estimated \$2.5M over purchase at current prices and eliminates procurement delay.

**No-cost Accelerator Operation.** The synchrotron today fills the CESR storage ring with  $e^+$  and  $e^-$  for x-ray production, and the experiment proposed here will operate entirely in the shadow of the x-ray program, providing positrons for dark photons only in the 3-minute intervals between positron top-ups carried out for the x-ray program. Inefficiency due to toggling between two modes of operation is covered by an 80% duty factor. Under this plan there is no cost in this proposal for accelerator operations, thus saving an estimated \$2.3M for  $10^7$  seconds of beam time.

**Projected Performance.** The anticipated performance of MMAPS is based on GEANT4 simulation [19]. The sensitivity is shown in Fig. 1, which indicates the region of the parameter space of coupling constant versus mass that this experiment can exclude at  $2\sigma$  or  $5\sigma$  with a run of  $10^7$  seconds, together with the existing set of exclusion limits from other experiments. MMAPS out-

performs all other experiments by a wide margin in the mass range 10-70 MeV and covers a large area of unexplored parameter space.

### 1.3 Results from Prior NSF Support

The preliminary results described here were obtained with NSF support via grant NSF-PHY-1446993, “EAGER Proposal: Preliminary Studies for a Dark Photon Search” (7/1/14-6/30/15), (Alexander, Perelstein, Rubin, Wittich), \$32,913. The **Intellectual Merit** is contained in this document: the design of this dark matter experiment. The **Broader Impacts** were that this work was carried out by undergrads, teaching them dark matter physics, tools (GEANT, ROOT) and experiment design. Perelstein is also supported under NSF-PHY-1316222, “Elementary Particle Theory”, (01/01/14-07/31/17), \$1,040,000. **Intellectual Merit:** the project investigated a variety of dark matter candidates and their experimental signatures, and interpretation of dark matter search results in terms of particle physics models [20–26]. **Broader Impact:** The results have been presented at many conferences, and provided graduate student training. Alexander and Wittich are supported under NSF-PHY-1307256 and its precursor, “Particle Physics at the Energy Frontier” (9/01/13-8/31/16) \$4,100,000. **Intellectual Merit:** Searching for physics beyond the Standard Model confronts fundamental symmetries, the nature of mass, the dimensionality of space, and the cosmological origins of our universe [27–45]. **Broader Impacts:** Many papers, conference talks, seminars; bringing the challenge and excitement of LHC physics into our extensive program of outreach to K-12 students and teachers and the general public. Rubin is supported under NSF-PHY-1416318, “Cornell Program for Student-Centered Accelerator Science” (9/01/14-8/31/17) \$10,972,786, and its precursor “Lepton Collider R&D”. **Intellectual Merit:** Investigate physics of ultra-low emittance beams in electron and positron storage rings [46–51]. **Broader Impact:** Training for accelerator physics students and design of colliders for HEP and high brightness synchrotron light sources. Kubota has had no NSF support in the past five years.

## 2 Cross Sections and Kinematics

For positrons of energy  $E_+$  and electrons at rest in the lab, the center-of-mass energy of the collision  $\sqrt{s} = \sqrt{2m_e(m_e + E_+)} \approx \sqrt{2m_e E_+}$  determines the maximum  $A'$  mass that can be probed in a given experiment:  $M_{A'}^{\max} = \sqrt{s}$ . For  $E_+ = 5.3$  GeV,  $M_{A'}^{\max} = 73.6$  MeV.

The fundamental challenge for MMAPS is to find a small dark photon signal in the presence of much larger QED backgrounds. The key observable to discriminate signal and background is the invariant mass of the system recoiling against the photon, which can be reconstructed from the photon energy  $E_\gamma$  and scattering angle  $\theta_\gamma$  measured in the calorimeter. We will refer to this observable as “missing mass”,  $M_{\text{miss}}$ ; it is frequently more convenient to work with  $M_{\text{miss}}^2$ . In the limit of small angles ( $\theta_\gamma \ll 1$ ) and high beam energy ( $m_e/E_+ \ll 1$ ) it can be written as

$$M_{\text{miss}}^2 \equiv (p_{e^+} + p_{e^-} - p_\gamma)^2 \approx 2m_e \left( E_+ - E_\gamma \left( 1 + \frac{E_+}{2m_e} \theta_\gamma^2 \right) \right). \quad (2)$$

For signal events,  $M_{\text{miss}}^2 = M_{A'}^2$ . The important backgrounds either have  $M_{\text{miss}}^2 = 0$ , in the case of the  $\gamma\gamma$  background; or are broadly distributed in  $M_{\text{miss}}^2$ , in the case of radiative Bhabha, bremsstrahlung,  $3\gamma$ , and inelastic backgrounds. Backgrounds may also exhibit  $M_{\text{miss}}^2 < 0$ . The basic experimental strategy is to search for a bump on top of a smooth background in  $M_{\text{miss}}^2$ .

### 2.1 Backgrounds and Simulation

To evaluate the feasibility and reach of the proposed experiment, Monte Carlo simulations of the signal and all relevant background processes have been performed. The fundamental processes are

Table 1: Cross sections of background processes within the acceptance of the detector. For illustration, the signal cross section for  $M_{A'} = 50$  MeV and  $\alpha' = \alpha$  is also listed. The signal cross section scales linearly with  $\alpha'$ . Bremsstrahlung cross section (BS) is reported per target electron.

process	$e^+e^-$	$e^+e^-\gamma$	$2\gamma$	$3\gamma$	BS	Inel.	Signal ( $M_{A'} = 50$ MeV, $\alpha' = \alpha$ )
$\sigma(2^\circ\text{-}5^\circ)$ , $\mu\text{b}$	1500	160	44.2	12	13.6	< 1	110
Source	MG	MG	GEANT4	MG	Ref. [53]	GEANT4	Eq. (3)

simulated using MadGraph (MG) [52] and GEANT4 [19] software packages. The beryllium target, CsI calorimeter, other detector apparatus (see Sec. 4.4), and local environment are modeled with GEANT4; simulation includes effects of clustering and photon pileup. The main results of the MC study are summarized in Table 2.1 and Fig. 2, together with the sensitivity reach indicated in Fig. 1.

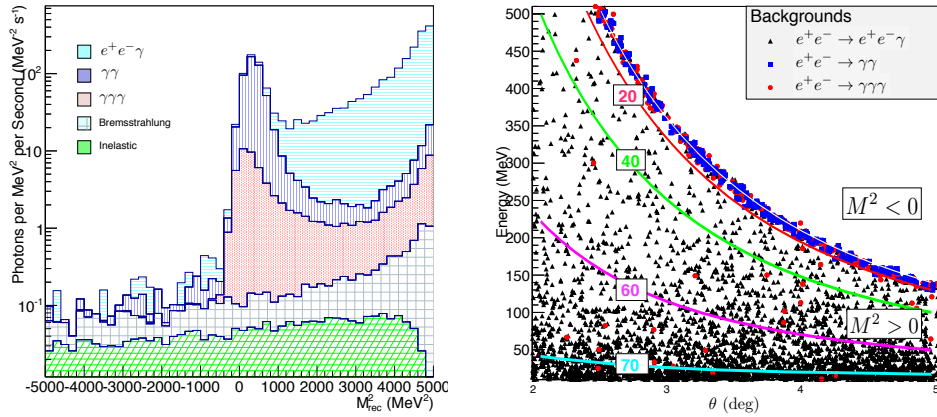


Figure 2: Left:  $M_{\text{miss}}^2$  spectrum for the main backgrounds:  $2\gamma$  (dark-blue),  $e^+e^-\gamma$  (cyan),  $3\gamma$  (red). Right: Distribution of background photons in the energy-vs-angle plane. Curves of constant  $M_{\text{miss}} = 0, 20, 40, 60, 70$  MeV shown in white, red, green, violet, and cyan. The  $M^2 < 0$  region is unpopulated due to limited statistics in simulation;  $E_{\text{beam}} = 5000$  MeV in both cases.

The cross section for the signal process,  $e^+e^- \rightarrow \gamma A'$ , is given by

$$\frac{d\sigma}{dx} \approx \frac{\alpha'}{\alpha} \frac{\pi r_0^2}{\gamma_+ x} \frac{(\mu + x)^2 + (1 - x)^2}{1 - x - \mu}, \quad (3)$$

where  $\alpha' = \varepsilon^2 e^2 / (4\pi)$ ,  $x = E_\gamma / (E_+ + m_e)$ ,  $\gamma_+ = E_+ / m_e$ ,  $\mu = M_{A'}^2 / (2\gamma_+ m_e^2)$ , and  $r_0 = \alpha / m_e \approx 0.282 \text{ bn}^{1/2}$  is the classical radius of the electron. To simulate the signal, we implemented this process in GEANT4; as expected, the signal events cluster around  $M_{\text{miss}}^2 = M_{A'}^2$ , with the width of the peak dominated by the experimental resolution.

There are six key backgrounds to consider:

1. Bhabha:  $e^+e^- \rightarrow e^+e^-$ . We suppress this large background with a dipole magnet immediately after the target; the magnetic field is set to sweep the low energy Bhabhas ( $< 700$  MeV) while

- the non-interacting ( $\sim 5$  GeV) beam stays within the central hole of the calorimeter.
2. Two-photon:  $e^+e^- \rightarrow \gamma\gamma$ . One hard photon goes down the central hole, the other is in the calorimeter acceptance. The event reconstructs with  $M_{\text{miss}} = 0$  because the unseen photon is a zero-mass object. We generate two-photon events with GEANT4 and confirm the GEANT4 results with a MadGraph check.
  3. Radiative Bhabha:  $e^+e^- \rightarrow e^+e^-\gamma$ . Most of the radiative Bhabha photons are soft in the center-of-mass frame of the  $e^+e^-$  collision, causing the background to peak near  $M_{\text{miss}} = \sqrt{s}$ . We generate events with MadGraph and propagate through the detector with GEANT4.
  4. Three-photon:  $e^+e^- \rightarrow \gamma\gamma\gamma$ . We generate the events with MadGraph and propagate them through the detector with GEANT4. A typical  $3\gamma$  event has one soft and two hard photons with kinematics similar to  $2\gamma$ , resulting in two peaks in the  $M_{\text{miss}}^2$  distribution, at 0 and  $s$ . One hard photon always goes down the central hole.
  5. Bremsstrahlung:  $e^+N \rightarrow e^+N\gamma$ . We generate events in GEANT4 using our own parametrization of the analytic bremsstrahlung formula [53], accurate to a few percent throughout the acceptance. Again, soft photons dominate, but overall this background is small.
  6. Inelastic:  $e^+N \rightarrow e^+\pi^0 X$ . We simulate these processes using GEANT4. We have validated GEANT4's low-energy inelastic models against old DESY [54] and SLAC [55] data and found GEANT4 to be accurate to about 20%. The inelastic processes produce a relatively flat recoil mass distribution, and their rate is completely subdominant.

### 3 Beam Extraction

To provide the positron beam needed for the MMAPS project we use the Cornell synchrotron [56]. The synchrotron accelerates both electrons and positrons to energies of approximately 5.3 GeV and in standard operating conditions transfers them to the CESR storage ring. From 1979 until 2008 the CLEO detector took data with CESR in colliding beam mode; today the ring is predominantly used for x-ray production. For MMAPS we will extract positrons from the synchrotron and deliver them to a fixed target; the acceleration and extraction take place between periodic fills for x-ray operations, ensuring efficient use of the machine without interference in x-ray production.

**Synchrotron Cycle.** Positrons are created and brought to 150 MeV in a short linac prior to injection into the synchrotron, where they are accelerated to 5.3 GeV. The average positron current in the synchrotron is  $I_{\text{avg}}^+ \sim 7.7$  nA. The synchrotron acceleration cycle repeats 60 times per second; the high energy beam is normally extracted at the peak of the ramp. The orbital period is 2.52  $\mu$ s, with 180 bunches at 14 ns intervals. Maximum positron current is realized in 15 bunches spaced 168 ns apart. A bunch completes  $\sim 3000$  turns from injection to extraction at the peak of cycle.

**Resonant Extraction.** For routine injection into the CESR storage ring, the entire beam in the synchrotron is extracted on a single turn by a fast kicker. For MMAPS operation, a slow spill is preferred to minimize pileup; we plan to use a resonant extraction scheme, whereby the synchrotron beam is slowly extracted over about 1000 turns ( $\sim 2.5$  ms). To accomplish this, quadrupoles shift the betatron tune of the synchrotron beam onto a third-integer ( $Q = 10\frac{2}{3}$ ), and a localized sextupole field drives a nonlinear resonance that shrinks the stable region of phase space in a controlled manner. The amplitude of the particles outside of the shrinking stable region increases over the course of several turns, until the horizontal displacement of particles outside the stable region is sufficient to clear a thin septum. Particles that clear the first thin septum receive a small transverse kick, sufficient to separate their trajectory from particles that remain in the accelerator. Two stronger septa then steer the particles into the extraction beam line. A resonantly extracted electron beam was used in fixed target experiments at Cornell in the period 1968-1979 [57] and is also in routine use today at the 3.5 GeV ELSA ring in Bonn [58] and at FNAL [59] for the Mu2e experiment.

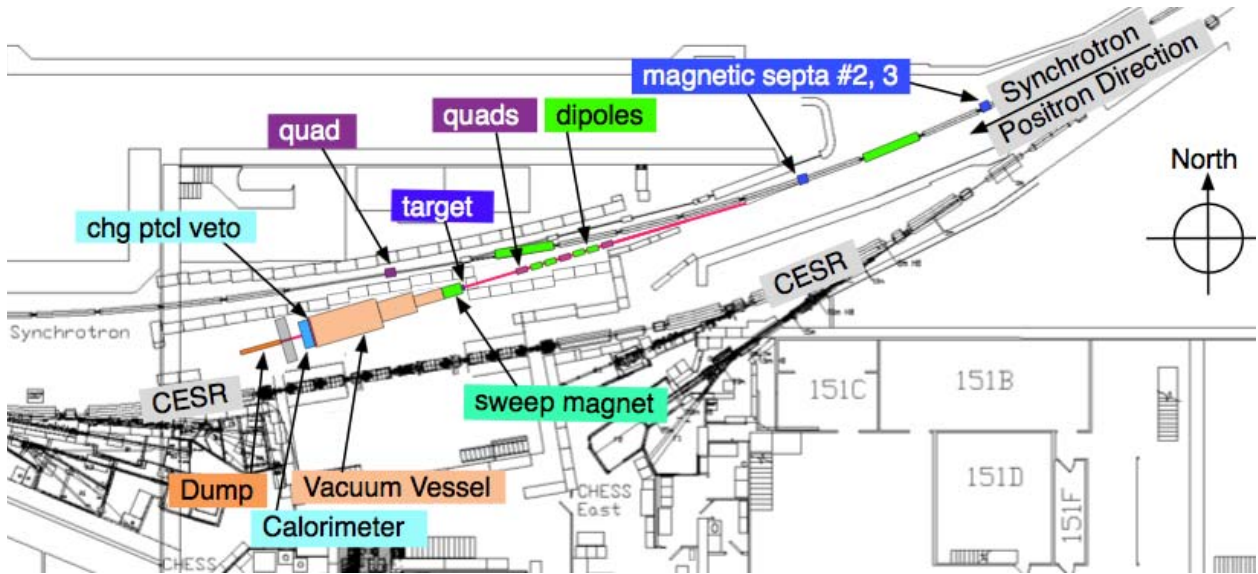


Figure 3: Approximate configuration of dark photon apparatus. Plan view shows south arc of synchrotron and CESR storage ring with MMAPS detector and beamline superimposed.

**Extraction Efficiency.** Extraction efficiency depends on our ability to manipulate the betatron tune of the synchrotron with quadrupoles, the strength of the resonance with the sextupole, and the performance of the extraction septa. Simulation studies indicate that the extraction efficiency will be around 80% with an 0.8 mm thick first septum, which is consistent with performance achieved under a similar extraction strategy in the pre-1979 era. For a fixed extraction efficiency, the emittance of the extracted beam scales with the thickness of the first septum; the simulations show that the extracted beam emittance is well below the experimental requirement, even with a 1 mm first septum. To minimize the emittance of the extracted beam, the high energy beam is moved to within  $\sim 10$  mm of the septum with a 3-component pulsed bump that turns on at the start of the extraction cycle. Evolution of the phase space of the positron beam through acceleration cycle is shown in Fig. 4.

**Magnets and Septa.** The capability to resonantly extract beam from the synchrotron requires installation of a new sextupole and two quadrupole magnets, together with associated current sources. A single sextupole will drive the resonance. One trim quadrupole will be needed to shift the horizontal betatron tune onto the resonance and another to fix the vertical tune. To move the beam close to the first septum for extraction, a closed-orbit bump is generated with the existing trim windings on three of the synchrotron magnets. The uniformity with which positrons are extracted through the  $\sim 1000$  turn extraction cycle is sensitive to the tune shift (controlled by the quadrupole), the sextupole strength, and the bump amplitude from one turn to the next. Programmable power supplies for the extraction magnets will enable the requisite fine tuning.

The first septum is relatively thin ( $\lesssim 1$  mm). Its kick of about 0.5 mrad separates the outgoing particles from the circulating beam so that they clear a second, stronger septum, with a thickness of about 6 mm. The first and second septa are both radially inside of the synchrotron stable orbit. The second septum kicks the beam into the aperture of a third septum, located radially outside the stable orbit, which then directs the beam into the extraction line. The second septum kicks the beam into the aperture of a third septum, that is radially outside of the synchrotron orbit. The

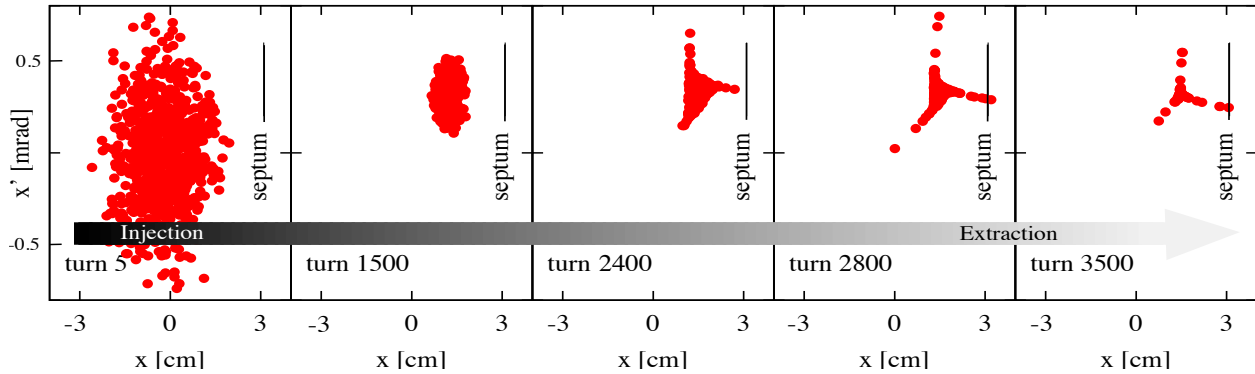


Figure 4: Beam phase space in the synchrotron at five points during the acceleration and extraction cycle. At injection from the linac into the synchrotron (turn 5, leftmost panel), the beam fills the phase space aperture. By turn 1500 the emittance has shrunk as the particles gained energy, and the bump has shifted the beam centroid towards the extraction septum. Around turn 2400, the pulsed quadrupole and sextupole shrink the stable phase space. During turns 2500-3500 (right two panels), the particles outside the stable region step beyond the septum and into the extraction line.

third septum directs the beam into the extraction line

**Power Supplies.** The sextupole, quadrupoles, and trim windings for the closed-orbit bump will all require programmable current sources, similar to those commonly used for optimizing waveforms of other synchrotron components. Uniform extraction over a thousand turns is sensitive to the proximity to the third integer resonance and the strength of the sextupole. The septa, on the other hand, can be powered in series with the synchrotron dipoles, in the same way that the septa are currently powered to extract beam for injection into CESR. The beam energy varies over the course of the extraction cycle, but at any given moment the synchrotron dipole magnetic field is precisely known, given the phase in the cycle, and the beam energy is fixed by the synchrotron  $\sim 1\%$  energy acceptance. A measurement of the synchrotron beam position, with the turn-by-turn capable beam position monitor, gives the beam energy to  $< 0.1\%$ . The magnets in the extraction beam line will likewise be powered in series with the synchrotron magnets in order to maintain energy independent focusing and steering of the extracted beam.

**Extracted Beam Line.** The beam line for the extracted beam will be outfitted with three quadrupoles, and two pairs of horizontal and vertical dipole correctors to steer and focus it onto the target. The quadrupoles will be assembled from the same laminations that were used to build existing synchrotron quadrupoles. The extraction line magnets will be powered in series with the synchrotron magnets so that the magnetic fields in the extracted beam line follow the beam energy. The dipole correctors will be air core (low impedance) magnets that permit near turn-by-turn correction of the varying launch angle of the extracted particles with programmable supplies.

**Synchrotron Simulation.** A model of the synchrotron guide field [61], including the magnets required for resonant extraction, was used to study resonant extraction. The time-dependent fields of the sextupole, quadrupole, and displacement bump magnets were tuned in the simulation to produce a nearly uniform spill, thus defining the required time dependence of the magnets. The integrated extraction rate as well as the time dependence of the extraction magnets is shown in Fig. 5(a). Fig. 5(b) shows the phase space of the extracted beam.

To benchmark the simulation results with measurements, we have recently installed a high band-



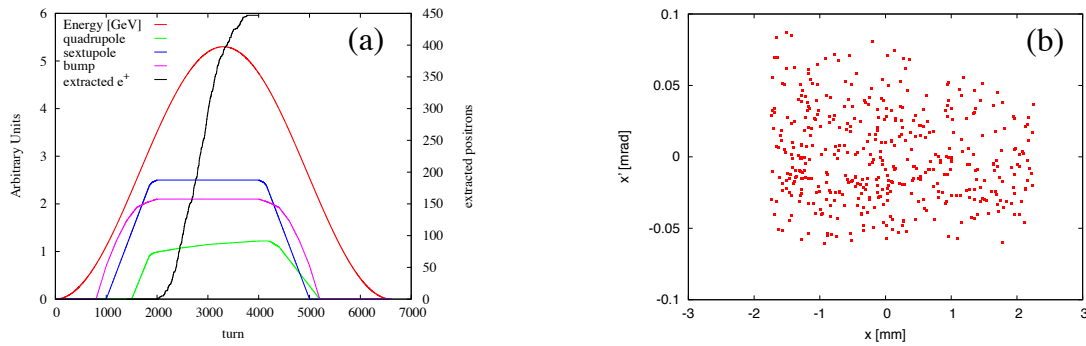


Figure 5: (a) The rate at which particles are extracted depends in detail on the bump amplitude (magenta), betatron tune (green) and sextupole strength (blue). The black curve is the corresponding cumulative sum of extracted positrons. (b) Phase space of extracted beam.

width stripline detector in the synchrotron to measure the turn-by-turn transverse position of the accelerating beam. The resulting turn-by-turn position spectra yield betatron (transverse) and synchrotron (longitudinal) tunes. The measured displacement corresponds to the turn dependent energy offset. We are preparing to install two additional strip line detectors near the extraction sextupole and septa, respectively, to measure betatron phase advance.

**Magnet Specifications.** To shift the betatron tunes onto the resonance we will use the existing quads outfitted with programmable shunts for coarse adjustment, and a new ferrite core quad for fine tuning. The ferrite quadrupole has poles assembled in the Panofsky style, and is wound with a two-turn coil to minimize inductance. It is therefore able to generate variations in magnetic field at the required time scale (see Fig. 5a) to provide fine adjustment of the tunes. The sextupole will be assembled from ferrite and excited with a six turn coil.

The specifications for the second and third (thick) septa are identical to septa currently in service for extraction into the storage ring, while the first, thin septum, is designed specifically for this application. We will use thin laminations and a single turn coil with septum thickness 0.8 mm. A thin septum (1 mm or less) gives extraction efficiency  $> 80\%$  and emittance of the extracted beam  $< 0.1$  mm-mrad, well below the experimental specification. The kick from the third septum will be sufficient to steer the positrons through a synchrotron magnet with an extraction channel. The magnet with extraction channel exists in our inventory.

Three synchrotron-style quadrupoles will be assembled for installation in the extraction line. Air or ferrite core dipole correctors will complete the complement of magnets in the external beam line. Finally, a fixed 1 m long dipole, shown in Fig. 6 will be placed immediately beyond the target to sweep electrons and positrons created in the target out of the calorimeter acceptance.

**Operations.** The synchrotron will continue to serve as the injector for the storage ring for its primary role as an x-ray source. Every three minutes the delivery of positrons to the MMAPS target will be interrupted for top-off of the positron beam in the storage ring; this will result in a duty cycle for MMAPS operations of 80%. We also anticipate that with a conservative design of the components for the resonant extraction scheme, we will extract  $\sim 30\%$  of the positrons produced in the linac, corresponding to an average current  $\langle I_+ \rangle \sim 2.3$  nA.

### 3.1 The External Beam

**Requirements on beam phase space at target.** A measurement of the missing mass,  $M_{\text{miss}}^2 \equiv (p_{e^+} + p_{e^-} - p_\gamma)^2$ , requires knowledge of both the final and initial state kinematics. The

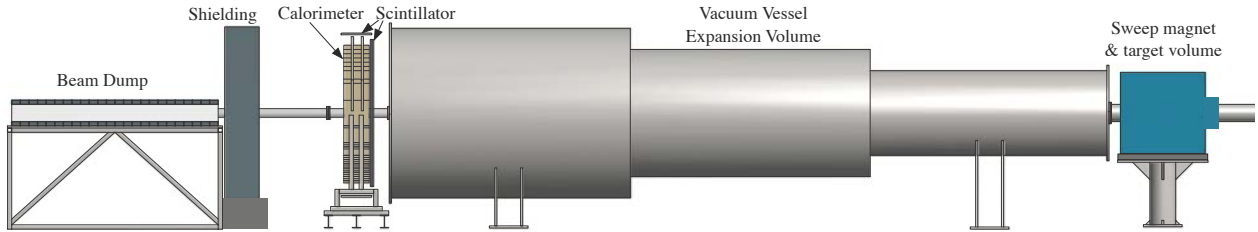


Figure 6: Elevation view of MMAPS.

extraction system described above will provide an incoming positron beam whose energy, direction, and position lie well within the specifications,  $\sigma_{E_+} < 15$  MeV,  $\theta_+ \ll 0.4$  mrad, and  $\sigma_x, \sigma_y \ll 4$  mm. For beam parameters within these limits, the spread in beam phase space has no discernible impact on missing mass resolution.

**Diagnostics & monitoring.** The beam extracted from the synchrotron needs to be steered to the target. The fast BPMs will be used for tuning the beam extraction and monitoring the pass through the exit beam line. We plan to use four beam monitors in the vacuum channel between the accelerator and production target and an additional one in front of the beam dump. Each monitor will be of the “SciFi” type [62] and will have 64 scintillating fibers with multianode PMT readout [63]. With slight modifications, we can use an existing data acquisition system to feed the beam position and size data to the accelerator control system. The monitor with a sensitive area 3.2 cm by 3.2 cm, shown in Fig. 7, will be inserted into the beam path for the period of observation via remote control and retracted when not in use. The multianode PMT is situated outside the beam vacuum. The insertion/retraction mechanism will allow a 50 mm stroke using a commercial Lesker mechanism [64].

**Luminosity.** The 2.5 msec beam spill repeats every  $\frac{1}{60}$  sec = 16.7 msec, and each spill is further substructured into 15,000 bunches, uniformly spaced by 168 ns; each bunch delivers about 17,000 positrons to the target. Given a beryllium target of 12.7 mm length, the luminosity can be calculated. We distinguish between the *average* luminosity, which determines final statistical sensitivity for the experiment, and the *peak* luminosity, which drives the occupancy in the calorimeter during the spill:

$$\mathcal{L}_{\text{av}} = 0.9 \times 10^{34} \text{ cm}^{-2} \text{ s}^{-1} \qquad \mathcal{L}_{\text{pk}} = 6.1 \times 10^{34} \text{ cm}^{-2} \text{ s}^{-1}. \quad (4)$$

## 4 Detector

The extracted beam line directs the positrons onto the beryllium target, and a calorimeter sitting 10 m further downstream measures the energy and direction of photons produced by the  $e^+e^-$  collisions. The experimental setup, illustrated in Fig. 6, includes a large vacuum vessel between the target and calorimeter, a scintillator veto wall to exclude charged particles, and a beam dump. The vacuum window at the calorimeter is  $0.015 X_0$  thick. The active area of the calorimeter and veto wall covers a solid angle of  $2^\circ - 5^\circ$  in the lab frame (roughly  $137^\circ - 162^\circ$  in the CM frame).

### 4.1 Calorimeter

The CLEO CsI calorimeter [65–69] will be reconfigured to serve as the MMAPS calorimeter. While it was designed for photons in the energy range 30–3000 MeV, and for CLEO’s relatively low-rate environment, the photon energies in MMAPS lie in the lower range 5–700 MeV and need to be measured in high-rate conditions. These differences lead us to replace the CLEO photodiodes with photomultiplier tubes (PMTs); no other significant changes are planned.

**Configuration.** The calorimeter is a stack of CsI crystals located 10 m from the target; see Figs. 6 and 7. The crystals, recovered from the CLEO endcap calorimeters, are  $5 \times 5 \times 30 \text{ cm}^3$  rectangular solids, well suited to stacking in simple arrays. The inner and outer radii of the annular configuration correspond to lab angles  $2^\circ \lesssim \theta_\gamma \lesssim 5^\circ$ . The angle  $\theta_\gamma$  measures the direction of the photon with respect to the beam axis. For the dimensions given above, the total number of crystals needed is about 700, roughly half the number of crystals in the CLEO endcaps. The crystals are wrapped with a thin layer of white teflon film, which, enhanced by a backing of aluminized mylar, serves as a diffuse (Lambertian) scatterer.

**Crystals & Readout.** The Thallium-doped CLEO CsI crystals have a high scintillation yield of 54,000 photons per MeV. The emission spectrum peaks around 560 nm, with a rise time of  $\sim 30 \text{ ns}$  and fall time of  $\tau \approx 1 \mu\text{s}$  [70]. In CLEO the CsI was read out with photodiodes, which could operate in magnetic field, required little space, and needed a relatively long shaping time to achieve the required noise performance. In MMAPS, the calorimeter is not in a magnetic field, space is not an issue, the typical photon energies are lower, and the high flux rate required by a search for rare phenomena demands faster response. Thus we have chosen to use PMTs.

The particle identification system in the Babar [71] experiment depended on fast, high-gain, low-noise PMTs [72]. The tubes are currently in storage at Jefferson Laboratory, and lab management has agreed to loan 1200 tubes for MMAPS at no cost (see accompanying letter in Supplemental Documents). For the emission spectrum of CsI(Tl), the Babar tubes have a quantum efficiency of 8% which, together with the photon collection efficiency of the crystal+tube system, leads to a photoelectron yield of 600 p.e. per MeV. A typical 15 MeV deposition in one crystal will therefore be measured with 1% precision (*i.e.* limited by photoelectron statistics), yielding an order of magnitude improvement over photodiode performance. Furthermore, the fast response of the PMT guarantees that it tracks the CsI(Tl) signal rise time without distortion, a feature that plays a crucial role in managing signal pileup.

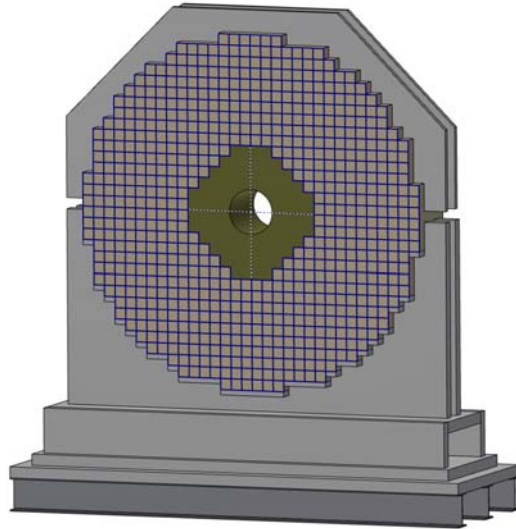


Figure 7: Front view of crystal calorimeter.

**Status of Crystals.** To determine the current state of health of the CLEO CsI, we have examined 64 crystals recovered from the CLEO endcap with cosmic ray events triggered by a small scintillator hodoscope. The minimum-ionizing deposition in 5 cm crystal thickness provides a signal source whose Landau peak at 28 MeV is well matched to the low end of the signal photon energy range in the dark photon experiment. Fig. 8 (left) shows a typical pulse height distribution. All crystals tested so far have been found to be within performance specifications.

**Resolution.** Photon energy resolution is the dominant contributor to the missing-mass resolution over most of the angular acceptance. The low intrinsic noise of PMTs ensures that electronic noise (a significant consideration for low energy photons in CLEO) is a minor contribution in MMAPS. In the 5-700 MeV range of interest, shower leakage out the back of the crystal is also not important. Thus side-leakage, due the lateral spread of the shower and the consequent fluctuation in energy recovered by clustering, dominates photon energy resolution.

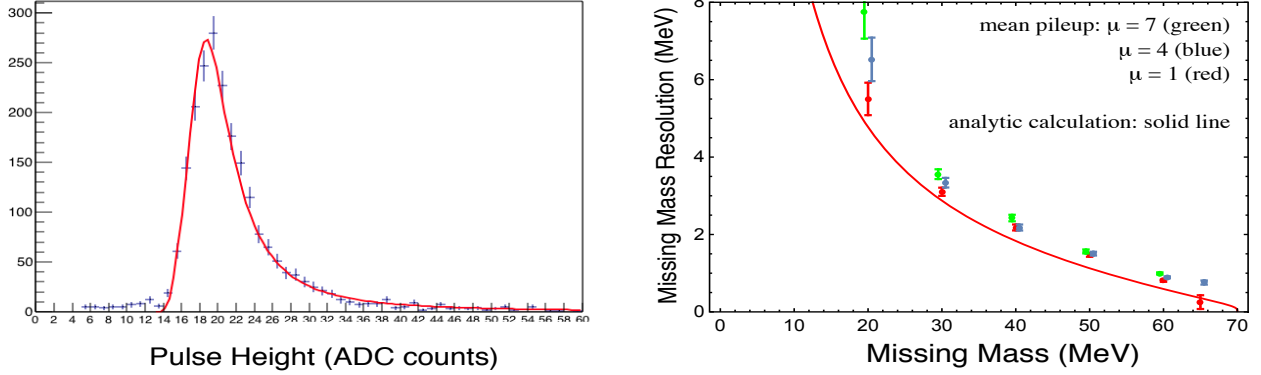


Figure 8: Left: Typical pulse height distribution in cosmic ray crystal test. (1 ADC = 1.5 MeV) Right: Resolution of missing-mass,  $\sigma_M$ . The points are from the full GEANT4 simulation with clustering implemented and a mean pileup as shown. Expected mean pileup is  $\mu = 2.2$ .

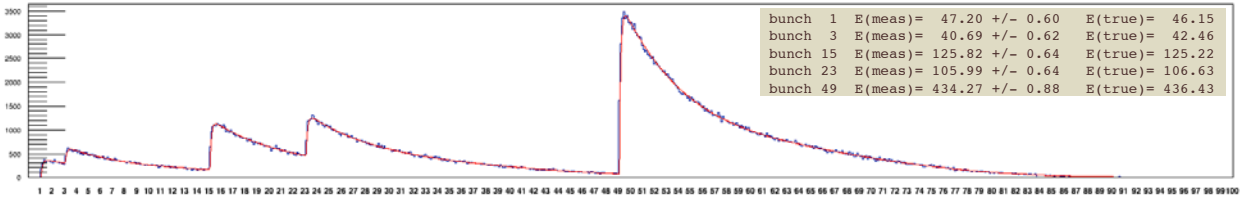


Figure 9: One-crystal waveform after digitization, for 100 beam bunches (16  $\mu$ s). Vertical axis is in photoelectrons per 20 ns bin; successive beam bunches are separated by 8 bins. Signal fluctuations are due to photoelectron statistics.

An additional contribution comes from signal pileup, when two or more photons deposit energy in the same crystal in nearby beam bunches. The PMT outputs will be continuously digitized by FADCs, and the resulting waveforms analyzed to extract individual photon energies and arrival times. Fig. 9 shows a sample waveform from 16 microseconds of simulated data, showing 5 pulses in one crystal. (The waveform shown is chosen to emphasize extreme pileup conditions: for nominal operating conditions,  $\mu = 2.2$ , a random sampling of 16  $\mu$ s of data has less than 1% chance of yielding 5 or more pulses.) Decomposing such a pulse train into individual hits is done by an algorithm that takes advantage of the fixed pulse shape and discrete arrival times. The sharp rise of the signal is an important feature for detecting the start of a new pulse.

The average amount of photon pileup is determined by the peak luminosity, the 1  $\mu$ s characteristic time profile of CsI(Tl) emission, and the background cross sections, acceptances, and spatial distributions. For the intended running conditions, *i.e.* the peak luminosity as given in Eq. 4, we find the average number of photons in the calorimeter for any beam bunch is  $\mu = 2.2$ .

The missing mass resolution, with all of the above effects included in the simulation, is shown in Fig. 8 (right). For reference, a simplified analytical calculation of the expected resolution is also shown.

## 4.2 Waveform Digitization and Pulse Reconstruction

**Waveform Digitization.** Each PMT produces a continuous output that is digitized by an FADC and processed for signal recognition and zero suppression in the local FPGA. The board for this has

been developed by the Mu2e experiment at Fermilab [73], and we are using a prototype at Cornell in developing this proposal; the plan is to use the same design for the final detector, slightly optimized for MMAPS requirements. Signals are digitized at a rate of 50 MS/s with minimal bandwidth limiting at the frontend to suppress aliasing. Fig. 10 shows the digitized output from two piled-up signals; the second pulse is delayed to arrive 168 ns after the first to simulate the beam pulse separation. The time resolution is clearly adequate to disentangle closely spaced signals.

Each frontend board has 16 ADC channels. Six frontend boards are interconnected for readout via a readout controller (ROC) that has two 2.5 Gbps fiber links, one for clock distribution and control and one for data readout. In our application, we use the ADCs in streaming mode, with the FPGA doing edge-finding and integration of pulses, with zero suppression. To instrument 700 crystals plus spares, we would require approximately 50 frontend boards and 10 readout controllers. The data is sent via the ROC for offline processing and further data reduction. Prototype versions of these boards are in existence and are being used at Fermilab for detector development and prototyping.

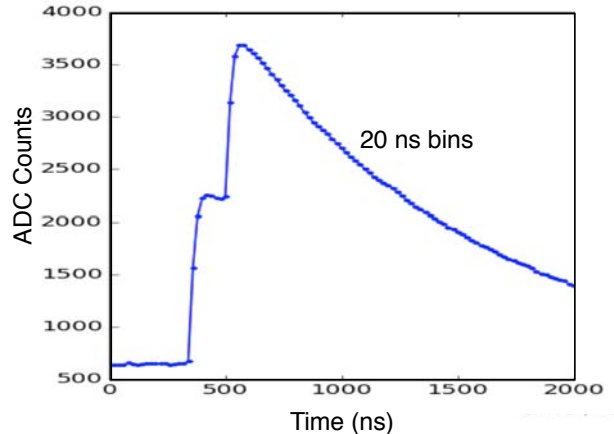


Figure 10: Observed ADC output for two pulses with 168ns separation.

**Data Handling.** At nominal luminosity, the average occupancy of the detector is  $\mu \approx 2.2$  photons per beam bunch on target. After online processing in the FPGA, average data transmission from the detector will be  $\sim 15\text{MB/s}$ , with a peak rate of  $\sim 100\text{MB/s}$ . A fiber with 1 Gbps capacity will transfer the data for offline processing. One year of data taking will generate  $\sim 100$  TB of raw data, which will be stored with a mix of disk and tape media. For online data quality monitoring and offline processing we plan to use the Fermilab-supported *art* framework [75].

### 4.3 Dealing with Charged Particles

Not everything that strikes the calorimeter is a photon. Charged particle sources include Bhabha production;  $e^+e^-$  from photon conversions in the 0.03-radiation-length target; and secondary charged debris from photons and charged particles striking the shielding walls, the floor, the vacuum vessel, or back-scattering off the beam dump. Cosmic muons are also a small source. We implement the following controls on charged particles.

**Sweeping magnet.** For Bhabha production in the target, we place a sweeping magnet immediately after the target. With a field integral of 0.2 T-m, the magnet sweeps lower energy charged particles out of the calorimeter acceptance while leaving the high-energy component of non-interacting beam inside the central beam hole.

**Veto wall.** Secondary debris created after the sweeping magnet is vetoed by a scintillator hodoscope covering the face of the calorimeter. The array consists of 324 slats of 1/2-inch plastic scintillator (EJ-200), instrumented with Babar PMTs. The PMTs are read out through the same digitization electronics as in the calorimeter, thus keeping the DAQ system homogeneous. The slats are organized in both horizontal ( $x$ ) and vertical ( $y$ ) arrays.

**Cosmic tagger.** The scintillator array includes two horizontal components, a “ceiling” above and “floor” below the calorimeter, which will be used to tag cosmics. The  $\sim 300$  Hz cosmic rate is negligible compared with the 6 MHz beam bunch rate, and the long tracks are easily eliminated

by pattern recognition during analysis, but cosmic muons provide a useful sample for calibration which will be discussed in the next section.

**Dump shield.** Backscattered debris from the beam dump, is absorbed in a 24-inch thick concrete wall. Leftover steel from the CLEO magnet may also be used.

#### 4.4 Calibration

Calibration constants that convert ADC counts to MeV must be measured precisely and frequently. Several independent methods allow for plenty of cross-checking; the list below covers three key methods, but is not exhaustive.

**Two-gamma calibration.** In  $e^+e^- \rightarrow \gamma\gamma$  events, only one photon is in the calorimeter acceptance, and its angle  $\theta_\gamma$  is correlated with its energy:  $E_\gamma = m_e/(1 - \beta_{CM} \cos \theta_\gamma)$ . The calorimeter geometry will be known to arbitrary precision, allowing us to use the measured angle to determine energy with a resolution  $\sigma_E = |dE/d\theta|\sigma_\theta$ . In practice  $\sigma_\theta \approx 1$  mrad, and  $|dE/d\theta|$  varies with angle from 3 MeV/mrad to 36 MeV/mrad. This calibration achieves a precision well below the intrinsic resolution single-photon resolution: a few seconds of data is sufficient to calibrate every crystal to a fraction of a percent accuracy at the particular energy corresponding to the crystal's position.

**Cosmic calibration.** Each crystal in the calorimeter sees a  $\sim 2$  Hz rate of cosmic rays. The most probable value of the energy deposition for a 5 cm path length in CsI is 28 MeV. The actual path length will vary but can be accurately determined event-by-event by using the full crystal array and the two horizontal scintillator layers for tracking. With one day of cosmic tracks, the peak of the Landau distribution can be determined in every crystal to better than 0.5%. This provides a calibration at a fixed low energy point.

**Beam calibration.** The sweeping magnet plays two roles, the main one being to sweep Bhabhas out of the calorimeter acceptance. The second is to steer low-current, low-energy beam, provided during dedicated calibration runs, at selected crystals. Independently controlled horizontal and vertical coils allow one to choose the  $(\phi, \theta)$  direction to strike a selected crystal. This provides absolute calibration across the middle range of energy; but the process is slow and will be done infrequently.

#### 4.5 Beam Dump

The noninteracting beam is absorbed in a dump located downstream from the calorimeter (see Fig. 6). Except for the target, the beam remains in vacuum until reaching the dump. Additional shielding, not shown in Fig. 6, will surround both the target, to limit extraneous radiation, and the calorimeter, to suppress unwanted background radiation from the dump and nearby accelerators. Cooling is handled by convection to the air as the total beam power is only 12 W. The dump consists of an  $8'' \times 8'' \times 8'$  block of aluminum, with two-inch thick lead bricks on three sides. The longitudinal depth of the dump corresponds to 27.4 radiation lengths. The beam dump has been fully simulated with MCNPX v27a [74] to assess the design for radiation safety; it passes all requirements.

### 5 Timetable.

For planning purposes, we divide the proposed 3-year project into 12 quarters.

**Accelerator Activities.** During Quarters 1, 2, and 3 we carry out the magnet and power supply procurement and fabrication, and design and fabricate the vacuum components. Work on the synchrotron is limited to scheduled downs in June, July, and January. In the first summer we reconfigure shielding blocks and complete the dismantling of CLEO. In the 4th quarter, we test magnets, program power supplies, fabricate magnet support structures, and interface the SciFi

diagnostics to the machine control system. Magnet installation and synchrotron reconfiguration occurs in 5th quarter. Accelerator control software modifications begin also in the 5th quarter, and in the 6th quarter we test the beam extraction protocols. Remaining work in the synchrotron tunnel is completed in the 2nd January down; synchrotron recommissioning is in the 7th quarter.

**Experiment Activities.** In Quarters 1 and 2 we select and test crystals and PMTs, fabricate the calorimeter support structure, and procure/fabricate electronics. In Quarter 2 through 6 we write FPGA firmware, do full-system electronics testing, write DAQ software, followed by calibration and online monitoring and control software in Quarter 6. Calorimeter and veto assembly begin in Quarter 3, with installation and testing in Quarters 4 and 5, and a cosmic ray shakedown run beginning immediately after. Commissioning and running begin in Quarter 8.

## 6 Division of Responsibilities

The senior personnel are well-suited to carry out this research, with experts in accelerator physics (Rubin), instrumentation (Kubota, Alexander, Wittich, Wojtsekhowski), theory of dark matter (Perelstein) and data analysis (all) on the team. Specific experience includes: the Cornell synchrotron (Rubin), magnet design (Rubin, Wojtsekhowski), CsI calorimetry (Kubota, Alexander), other calorimetry (Wojtsekhowski), frontend electronics (Kubota, Alexander), data acquisition and trigger (Wittich), and other dark photon searches (Wojtsekhowski).

Rubin will be responsible for the synchrotron modifications, commissioning, and operations. Rubin and Alexander will oversee the engineering and fabrication of magnets and power supplies and vacuum elements, as well as general mechanical engineering and materials handling needed for the synchrotron reconfiguration. Kubota will be responsible for CsI calibration, monitoring, and environmental control; Alexander for calorimeter frontend readout and charged particle veto; Wittich for backend electronics and DAQ; Wojtsekhowski for the design of the sweeping magnet and the SciFi beam monitor, and the Babar PMTs. Alexander and Wittich will jointly oversee the engineering and fabrication of electronics components. Perelstein is responsible for calculations, theoretical input, and Monte Carlo generators. All will take part in data analysis.

## 7 Broader Impacts of the Proposed Work

- **Accelerator R&D** The resonant extraction design, implementation, and commissioning is a project well suited to students of accelerator physics. Indeed, the concept outlined in this proposal is mainly the work of a Cornell graduate student. Students will develop the simulations to study dependencies, contribute to the design and testing of the accelerator equipment, participate in the machine studies to measure the properties of synchrotron beams, commission the slow spill hardware, and develop tuning algorithms for optimizing performance. It will provide a student training opportunity that is truly the only one of its kind anywhere in the world.

- **Graduate Research in Particle Physics** We plan for 3 to 4 graduate students ( $2\frac{1}{4}$  FTE) to work on MMAPS, one of whom will write a PhD thesis on the dark photon results. A small experiment of this kind offers a unique opportunity for students to engage in every aspect of the experiment from design to final data analysis, an experience that is rare in the current era of large collaborations.

- **Undergraduate Research in Particle Physics** Undergraduates play a big role in Cornell HEP, and will do so in the MMAPS experiment. The detector simulation and R&D described in this proposal have been done entirely by undergraduates. Other recent undergraduates have gone on to top graduate schools, including Stanford (Liu, Nachman), Chicago (Story), Harvard (Miyake, Chung, Stone), MIT (Wang), UCSB (Dishaw), and others. Nachman also won the prestigious Churchill Scholarship and spent the 2012-13 year at Cambridge University.

## References

- [1] B. Wojtsekhowski, “Searching for a U-boson with a positron beam”, [arXiv:0906.5265](#)
- [2] S. Abrahamyan *et al.* [APEX Collaboration], “Search for a New Gauge Boson in Electron-Nucleus Fixed-Target Scattering by the APEX Experiment,” *Phys. Rev. Lett.* **107**, 191804 (2011) [[arXiv:1108.2750](#) [hep-ex]].
- [3] R. Essig, P. Schuster, N. Toro and B. Wojtsekhowski, “An Electron Fixed Target Experiment to Search for a New Vector Boson A’ Decaying to e+e-,” *JHEP* **1102**, 009 (2011) [[arXiv:1001.2557](#) [hep-ph]].
- [4] S. Ritz *et al.*, “Building for Discovery: Strategic Plan for U.S. Particle Physics in the Global Context”, Report of the Particle Physics Project Prioritization Panel (P5), [available online](#) (June 2014).
- [5] R. Essig, J. A. Jaros, W. Wester, P. H. Adrian, S. Andreas, T. Averett, O. Baker and B. Batell *et al.*, “Working Group Report: New Light Weakly Coupled Particles,” [arXiv:1311.0029](#) [hep-ph].
- [6] M. Pospelov, “Secluded U(1) below the weak scale,” *Phys. Rev. D* **80**, 095002 (2009) [[arXiv:0811.1030](#) [hep-ph]].
- [7] G. W. Bennett *et al.* [Muon g-2 Collaboration], “Final Report of the Muon E821 Anomalous Magnetic Moment Measurement at BNL,” *Phys. Rev. D* **73**, 072003 (2006) [hep-ex/0602035].
- [8] N. Arkani-Hamed, D. P. Finkbeiner, T. R. Slatyer and N. Weiner, “A Theory of Dark Matter,” *Phys. Rev. D* **79**, 015014 (2009) [[arXiv:0810.0713](#) [hep-ph]].
- [9] Plots courtesy of Rouven Essig; private communication.
- [10] R. Essig, J. Mardon, M. Papucci, T. Volansky and Y. M. Zhong, “Constraining Light Dark Matter with Low-Energy  $e^+e^-$  Colliders,” *JHEP* **1311**, 167 (2013) [[arXiv:1309.5084](#) [hep-ph]].
- [11] H. Merkel *et al.*, “Search at the Mainz Microtron for Light Massive Gauge Bosons Relevant for the Muon g-2 Anomaly,” *Phys. Rev. Lett.* **112**, no. 22, 221802 (2014) [[arXiv:1404.5502](#) [hep-ex]].
- [12] J. R. Batley *et al.* [NA48/2 Collaboration], “Search for the dark photon in  $\pi^0$  decays,” *Phys. Lett. B* **746**, 178 (2015) [[arXiv:1504.00607](#) [hep-ex]].
- [13] B. Aubert *et al.* [BaBar Collaboration], “Search for Invisible Decays of a Light Scalar in Radiative Transitions  $v_{3S} \rightarrow \gamma A_0$ ,” [arXiv:0808.0017](#) [hep-ex].
- [14] S. Adler *et al.* [E787 Collaboration], “Further search for the decay  $K^+ \rightarrow \pi^+ \nu \bar{\nu}$  in the momentum region  $P \leq 195\text{-MeV}/c$ ,” *Phys. Rev. D* **70**, 037102 (2004) [hep-ex/0403034].
- [15] A. V. Artamonov *et al.* [E949 Collaboration], “New measurement of the  $K^+ \rightarrow \pi^+ \nu \bar{\nu}$  branching ratio,” *Phys. Rev. Lett.* **101**, 191802 (2008) [[arXiv:0808.2459](#) [hep-ex]].
- [16] B. Batell, R. Essig and Z. Surujon, “Strong Constraints on Sub-GeV Dark Matter from SLAC Beam Dump E137,” *Phys. Rev. Lett.* **113**, 171802 (2014) [[arXiv:1406.2698](#) [hep-ph]].



- [17] B. Wojtsekhowski, D. Nikolenko, I. Rachek, “Searching for a new force at VEPP-3”, [arXiv:1207.5089](#)
- [18] Mauro Raggi, Venelin Kozhuharov, P. Valente, “The PADME experiment at LNF”, [arXiv:1501.01867](#)
- [19] S. Agostinelli *et al.* [GEANT4 Collaboration], “GEANT4: A Simulation toolkit,” *Nucl. Instrum. Meth. A* **506**, 250 (2003).
- [20] Y. J. Chae and M. Perelstein, “Dark Matter Search at a Linear Collider: Effective Operator Approach,” *JHEP* **1305**, 138 (2013) [[arXiv:1211.4008](#) [hep-ph]].
- [21] M. Perelstein and B. Shakya, “XENON100 implications for naturalness in the MSSM, NMSSM, and  $\lambda$ -supersymmetry model,” *Phys. Rev. D* **88**, no. 7, 075003 (2013) [[arXiv:1208.0833](#) [hep-ph]].
- [22] M. Perelstein and B. Shakya, “Fine-Tuning Implications of Direct Dark Matter Searches in the MSSM,” *JHEP* **1110**, 142 (2011) [[arXiv:1107.5048](#) [hep-ph]].
- [23] M. Perelstein and B. Shakya, “Antiprotons from Dark Matter: Effects of a Position-Dependent Diffusion Coefficient,” *Phys. Rev. D* **83**, 123508 (2011) [[arXiv:1012.3772](#) [astro-ph.HE]].
- [24] M. Perelstein and B. Shakya, “Dark Matter Identification with Gamma Rays from Dwarf Galaxies,” *JCAP* **1010**, 016 (2010) [[arXiv:1007.0018](#) [astro-ph.HE]].
- [25] M. Perelstein and B. Shakya, “Remarks on calculation of positron flux from galactic dark matter,” *Phys. Rev. D* **82**, 043505 (2010) [[arXiv:1002.4588](#) [astro-ph.HE]].
- [26] P. Konar, K. Kong, K. T. Matchev and M. Perelstein, “Shedding Light on the Dark Sector with Direct WIMP Production,” *New J. Phys.* **11**, 105004 (2009) [[arXiv:0902.2000](#) [hep-ph]].
- [27] N. Eggert, “Kinematic Endpoint Variables and Physics Beyond the Standard Model”, Ph.D. Thesis, Cornell University, 2014
- [28] CMS Collaboration, Cornell authors: J. Alexander, N. Eggert; “Searches for electroweak production of charginos, neutralinos, and sleptons decaying to leptons and W, Z, and Higgs bosons in pp collisions at 8 TeV,” *Eur. Phys. J. C* **74**, no. 9, 3036 (2014) [[arXiv:1405.7570](#) [hep-ex]].
- [29] CMS Collaboration; Cornell authors: J. Alexander, N. Mirman, N. Eggert, B. Nachman, A. Dishaw, “Measurement of masses in the  $t\bar{t}$  system by kinematic endpoints in pp collisions at  $\sqrt{s} = 7$  TeV,” *Eur. Phys. J. C* **73**, 2494 (2013) [[arXiv:1304.5783](#) [hep-ex]].
- [30] N. Mirman for CMS Collaboration; “Missing transverse energy significance at CMS”, Proceedings, 2nd Conference on Large Hadron Collider Physics Conference (LHCP 2014), [arXiv:1409.3028](#)
- [31] CMS Collaboration; Cornell authors: J. Alexander, N. Mirman, Y. Wang; “Performance of the missing transverse energy reconstruction by the CMS experiment in  $\sqrt{s} = 8$  TeV pp data”, [arXiv:1411.0511](#); submitted to JINST.

- [32] CLEO Collaboration; Cornell authors: J. Alexander, X. Shi, et al, “Updated measurements of absolute  $D^+$  and  $D^0$  hadronic branching fractions and  $\sigma(e^+e^- \rightarrow D\bar{D})$  at  $E_{\text{cm}} = 3774$  MeV,” *Phys. Rev. D* **89**, no. 7, 072002 (2014) [arXiv:1312.6775 [hep-ex]].
- [33] X. Shi, “Measurement of absolute hadronic branching fractions of  $D$  mesons”, Ph.D. Thesis, Cornell University (2011).
- [34] D. M. Puigh, “Search for a heavy gauge boson  $W'$  in the final state with an electron and large missing transverse energy in  $pp$  collisions at  $\sqrt{s} = 7$  TeV”, Ph.D. Thesis, Cornell University (2012).
- [35] S. T. Poprocki, “Search For  $WZ + ZZ$  Production With Missing Transverse Energy and  $b$  Jets at CDF”, Ph.D. Thesis, Cornell University (2013).
- [36] CMS Collaboration, Cornell Authors: Thompson, Winstrom, Teo, Kreis, Thom, Wittich, Kaufmann, and Ryd. “Search for supersymmetry in events with b-quark jets and missing transverse energy in  $pp$  collisions at 7 TeV”, *Phys. Rev. D* **86**, 072010 (2012) arXiv:1208.4859.
- [37] CMS Collaboration, Cornell Authors: D. Puigh and P. Wittich. “Search for a heavy gauge boson  $W$  in the final state with an electron and large missing transverse energy in  $pp$  collisions at  $\sqrt{s} = 7$  TeV,” *Phys. Lett. B* **698** 21 (2011).
- [38] CMS Collaboration, Cornell Authors: J. Thom, Y. Weng, H. Lui, S. Bannedsen, P. Wittich and D. Teo, “Measurement of the  $t\bar{t}$  production cross section in  $pp$  collisions at 7 TeV in lepton+jets events using b-quark jet identification”, *Phys. Rev. D* **84**, 092004 (2011).
- [39] CMS Collaboration, Cornell Authors: J. Alexander, N. Eggert, N. Mirman, A. Dishaw, B. Nachman; [CMS PAS PAS-TOP-11-027](#) (2011). Presented at the 5th International Workshop on Top Quark Physics, September 2012, Winchester, UK. Paper currently in preparation.
- [40] CMS Collaboration (S. Chatrchyan *et al.*), Cornell Authors: J. Alexander, L. Gibbons, A. Khukhunaishvili; “Determination of Jet Energy Calibration and Transverse Momentum Resolution in CMS,” *JINST* **6**, P11002 (2011) [arXiv:1107.4277 [physics.ins-det]].
- [41] CDF Collaboration, Cornell Authors: P. Wittich, S. Poprocki; “Search for  $WZ+ZZ$  production with MET + jets with b enhancement at  $\sqrt{s} = 1.96$  TeV”, *Phys. Rev. D* **85**, 012002 (2012).
- [42] J. Freeman, J.D. Lewis, W. Ketchum, S. Poprocki, S. Pronko, V. Rusu, and P. Wittich, “An artificial neural network based  $b$  jet identification algorithm at the CDF Experiment”, *Nucl. Instrum. Methods A* **663**, 37 (2011).
- [43] CDF Collaboration, Cornell Authors: P. Wittich, P. Kittiwisit; “Search for New Physics in High  $p_T$  Like-Sign Dilepton Events at CDF II”, *Phys. Rev. Lett.* **107** 181801 (2011).
- [44] J.P. Alexander, J. Thom, T. Lutz, M. Suri; “Interposer development for 3D trackers” presented at [Workshop on Intelligent Trackers](#), LBL, February 2010. Published in [Journal of Instrumentation](#) **5** C08008, 2010 doi: 10.1088/1748-0221/5/08/C08008
- [45] Peter Wittich *et al.*, “Applications of GPUs to Online Track Reconstruction in HEP Experiments”, IEEE NSS Conference, Anaheim, CA (2012).

- [46] J. R. Calvey, W. Hartung, Y. Li, J. A. Livezey, J. Makita, M. A. Palmer, D. Rubin, “Electron Cloud Measurements in Dipole, Quadrupole, and Wiggler Magnets,” Nucl. Instrum. & Methods A **770**, 141-154 (2015) <http://dx.doi.org/10.1016/j.nima.2014.09.069>
- [47] A. Chatterjee, K. Blaser, M. Ehrlichman, D. Rubin, J. Shanks, “Fast Ion Instability at CESR-TA,” in IPAC2014: Proceedings of the 5th International Particle Accelerator Conference, Dresden, Germany, edited by Christine Petit-Jean-Genaz, Gianluigi Arduini, Peter Michel, Volker R. W. Schaa, JACoW, Geneva, Switzerland, 2014, p. 1638-1640. <http://accelconf.web.cern.ch/AccelConf/IPAC2014/papers/tupri036.pdf>
- [48] J. P. Alexander, A. Chatterjee, C. Conolly, E. Edwards, M. P. Ehrlichman, E. Fontes, B. K. Heltsley, W. Hopkins, A. Lyndaker, D. P. Peterson, N. T. Rider, D. L. Rubin, J. Savino, R. Seeley, J. Shanks, J. W. Flanagan, “Vertical Beam Size Measurement in the CESR-TA e+e- Storage Ring Using X-Rays from Synchrotron Radiation,” Nucl. Instrum. & Methods A **748**, June 2014, p. 96-125. (arXiv:1311.6769)
- [49] J. Shanks, D. L. Rubin, D. Sagan, “Low-Emittance Tuning at the Cornell Electron Storage Ring Test Accelerator,” Phys. Rev. ST Accel. Beams **17**, April 2014, 044003. (arXiv:1309.2247)
- [50] M. P. Ehrlichman, A. Chatterjee, W. Hartung, B. Heltsley, D. P. Peterson, N. Rider, D. Rubin, D. Sagan, J. P. Shanks, S. T. Wang, “Measurement and Compensation of Horizontal Crabbing at the Cornell Electron Storage Ring Test Accelerator,” Phys. Rev. ST Accel. Beams **17**, April 2014, 044002. (arXiv:1311.1763)
- [51] M. P. Ehrlichman, W. Hartung, B. Heltsley, D. P. Peterson, N. Rider, D. Rubin, D. Sagan, J. Shanks, S. T. Wang, R. Campbell, R. Holtzapple, “Intrabeam Scattering Studies at the Cornell Electron Storage Ring Test Accelerator,” Phys. Rev. ST Accel. Beams **16**, October 2013, 104401. (arXiv:1308.0035)
- [52] J. Alwall, M. Herquet, F. Maltoni, O. Mattelaer and T. Stelzer, “MadGraph 5 : Going Beyond,” JHEP **1106**, 128 (2011) [arXiv:1106.0522 [hep-ph]].
- [53] Y. S. Tsai, “Pair Production and Bremsstrahlung of Charged Leptons,” Rev. Mod. Phys. **46**, 815 (1974) [Erratum-ibid. **49**, 521 (1977)].
- [54] C. K. Chen, J. Knowles, D. Martin, J. M. Scarr, I. O. Skillicorn, K. Smith, P. Joos and A. Ladage *et al.*, “Charged Hadron Multiplicities and Inclusive pi- Distributions in Inelastic e p Scattering,” Nucl. Phys. B **133**, 13 (1978).
- [55] S. Stein, W. B. Atwood, E. D. Bloom, R. L. Cottrell, H. C. DeStaebler, C. L. Jordan, H. Piel and C. Y. Prescott *et al.*, “Electron Scattering at 4-Degrees with Energies of 4.5-GeV - 20-GeV,” Phys. Rev. D **12**, 1884 (1975).
- [56] R. R. Wilson, “The 10-GeV TO 20-GeV Cornell Electron Synchrotron,” CS-33, NP-17179.
- [57] J. DeWire, H. Edwards, R. Littauer, G. Rouse and R. Sundelin, “An External Beam from the Cornell 10 GeV Synchrotron,” [Proceedings 1971 Particle Accelerator Conference](#), p. 964-965.
- [58] W. Hillert, “The Bonn electron stretcher accelerator ELSA: Past and future, Eur. Phys. J. A **28S1**, 139 (2006).

- [59] V. Nagaslaev, J. Amundson, J. Johnstone, L. Michelotti, C. S. Park, S. Werkema and M. Syphers, “Third interger resonance slow extraction scheme for a mu- $\epsilon$ e experiment at Fermilab,” arXiv:1207.6621 [physics.acc-ph].
- [60] Animation of beam phase space evolution in resonant extraction: <http://www.lns.cornell.edu/~dlr/darkphoton/resonantextraction4000.gif>
- [61] D. Sagan, Nucl. Instrum. Methods Phys. Res. A558, 356 (2006). [BMAD](#)
- [62] “A 1mm Scintillating Fibre Tracker Readout by a Multi-anode Photomultiplier” arXiv:1106.5649v1 [physics.ins-det] 28 Jun 2011
- [63] <http://www.hamamatsu.com/resources/pdf/etd/H8804.TPMH1333E.pdf>
- [64] [www.lesker.com](http://www.lesker.com)
- [65] Y. Kubota *et al.* [CLEO Collaboration], “The CLEO-II detector,” Nucl. Instrum. Meth. A **320**, 66 (1992).
- [66] E. Blucher, B. Gittelman, B. K. Heltsley, J. Kandaswamy, R. V. Kowalewski, Y. Kubota, N. B. Mistry and S. Stone *et al.*, “Tests of Cesium Iodide Crystals for an Electromagnetic Calorimeter,” Nucl. Instrum. Meth. A **249**, 201 (1986).
- [67] A. Bean, Z. Bian, J. Dobbins, K. Jim, J. Kandaswamy and N. B. Mistry, “On The Stability Of Low Leakage Silicon Photodiodes Used With Crystal Calorimeters,” IEEE Trans. Nucl. Sci. **33**, 411 (1986).
- [68] Z. Bian, J. Dobbins, and N. Mistry, “The Use of Silicon Photodiodes in a CsI(Tl) Calorimeter,” Nucl. Instrum. Meth. A **239**, 518 (1985). doi:10.1016/0168-9002(85)90030-0
- [69] Brian Heltsley “Three Lectures on the CLEO CsI” [Beijing Lectures](#)
- [70] J.D. Valentine, W.W. Moses, S.E. Derenzo, D. Wehe, G. F. Knoll, “Temperature dependence of CsI(Tl) gamma-ray scintillation decay time constants and emission spectrum” NIM A325 (1993) 147 [ScienceDirect link](#)
- [71] I. Adam *et al.* [BaBar DIRC Collaboration], “The DIRC particle identification system for the BaBar experiment,” Nucl. Instrum. Meth. A **538**, 281 (2005).
- [72] [EMI 9125FLB17, made by Electron Tube Ltd.](#)
- [73] [Mu2e Tracker Electronics \(CD2 Review\)](#)
- [74] MCNPX Users Manual, D. B. Pelowitz Ed., v.2.6.0, April 2006, LA-CP-07-1473, LANL
- [75] <https://web.fnal.gov/project/ArtDoc/Pages/home.aspx>